JAMES | Journal of Advances in Modeling Earth Systems

RESEARCH ARTICLE
10.1029/2018MS001399

A New Frozen Soil Parameterization Including Frost and Thaw Fronts in the Community Land Model

Junqiang Gao[1,2], Zhenghui Xie[1,3], Aiwen Wang[4], Shuang Liu[1,5], Yujin Zeng[1], Bin Liu[1,3], Ruichao Li[1,3], Binghao Jia[1], Peihua Qin[1], and Jinbo Xie[1]

[1]State Key Laboratory of Numerical Modeling for Atmospheric Sciences and Geophysical Fluid Dynamics, Institute of Atmospheric Physics, Chinese Academy of Sciences, Beijing, China, [2]School of Mathematics and Statistics, Nanjing University of Information Science and Technology, Nanjing, China, [3]College of Earth Science, University of Chinese Academy of Sciences, Beijing, China, [4]School of Applied Science, Beijing Information and Science Technology University, Beijing, China, [5]Key Laboratory of Mountain Hazards and Earth Surface Processes, Institute of Mountain Hazards and Environment, Chinese Academy of Sciences, Chengdu, China

Key Points:
- A new frozen soil parameterization including frost and thaw fronts was incorporated into version 4.5 of the Community Land Model
- Observed data from multiple sources were used to validate the performance of the new model in frozen ground simulation
- The model developed gave better performance than the original one in simulations of soil temperature and freeze-thaw processes

Correspondence to:
Z. Xie,
zxie@lasg.iap.ac.cn

Citation:
Gao, J., Xie, Z., Wang, A., Liu, S., Zeng, Y., Liu, B., et al. (2019). A new frozen soil parameterization including frost and thaw fronts in the Community Land Model. *Journal of Advances in Modeling Earth Systems*, *11*. https://doi.org/10.1029/2018MS001399

Received 9 JUN 2018
Accepted 14 FEB 2019
Accepted article online 18 FEB 2019

Abstract Freeze–thaw processes in soils, including changes in frost and thaw fronts (FTFs), are very sensitive to warming. However, the latest climate models do not predict changes in FTFs directly. In this study, a new frozen soil parameterization including changes in FTFs was incorporated into the Community Land Model version 4.5 for climate modeling, which we denote CLM4.5_FTF. A set of numerical experiments including single points, regions in China, and a global scale were conducted using the model to validate its performance. The simulated FTF depths compare well with observed data from both the D66 station (permafrost) and Hulugou station (seasonally frozen ground). The simulated active layer thickness, defined as the maximum thaw front depth in permafrost, is in general agreement but slightly greater than observations from the Circumpolar Active Layer Monitoring program. The simulated distributions of different types of frozen soil in China and permafrost in the northern hemisphere are in agreement with the frozen soil map of China and the International Permafrost Association map, respectively. The results confirm that the model performs well for FTF simulations. The model was also used for year-long simulations of soil temperature and freeze–thaw processes to check its applicability in continuous simulation. The results show that CLM4.5_FTF performed better than the original model, and the improvement was better for lower levels than for the upper level. Finally, we give simulated latent heat flux, sensible heat flux, and 10-cm soil temperature deviations determined via the couple model with and without the new scheme.

1. Introduction

Freeze–thaw processes in soils, including changes in frost and thaw fronts (FTFs), are important physical processes. The movement of FTF depths affects soil hydrothermal characteristics, while the soil thermal conductivity increases and the soil hydraulic conductivity decreases after the soil freezing. In turn, these affect the energy and water exchanges between the land surface and the atmosphere, and hydrothermal processes on the land surface. Soil frost depth influences the amount of snowmelt infiltration (Iwata et al., 2010; Zhang, 2005). Soil thaw depth is an important parameter because it affects the timing of cultivation and seeding in early spring (Harada et al., 2009). In addition, at locations where the uppermost permafrost is rich in ground ice, thickening of the active layer could have severe destabilizing effects on engineering works (Anisimov et al., 1997; Pang et al., 2009). Studies have shown that methane emissions will increase by 38% when the thickness of the active layer increases by 10 cm in the Arctic (Zhuang et al., 2004). The carbon storage capacity of permafrost in the Northern Hemisphere ecosystem is almost twice that of the atmosphere (Schuur et al., 2008, 2009; Zimov et al., 2006). Organic carbon deposited in permafrost begins to decompose and is gradually released into the atmosphere on permafrost ablation. Carbon entering the atmosphere eventually accelerates climate warming via a positive feedback loop (Schuur et al., 2009). Therefore, movement of soil FTFs impacts the terrestrial carbon cycle and thus the local climate and potentially the global climate. Long-term changes in FTF depths are an important indicator of climate change (Frauenfeld et al., 2004; Yi et al., 2006). The area of frozen soil accounts for approximately 50% of the Earth's surface, and permafrost occupies approximately 25% of the land area of the Northern Hemisphere (Zhang et al., 1999). In China, the area of frozen soil is equivalent to 75% of the land surface (Li et al., 2008). It is of primary importance to estimate FTF depth accurately because of the difficulty of observations in alpine and permafrost areas.

However, most land surface models, such as BATS (Dickinson et al., 1993), SSIB (Xue et al., 1996), SIB2 (Sellers et al., 1996), VIC (Cherkauer & Lettenmaier, 1999), SHAW (Flerchinger, 2000), CoLM (Dai et al., 2003), CoupModel (Jansson, 2012), and CLM (Oleson et al., 2013), tend to focus on the freeze–thaw cycle, and the FTF depth is often inadequately represented or even neglected. It is assumed that the phase transition occurs in the middle of each soil layer in these models, which will result in delayed or rapid freeze–thaw processes, especially in thick soil layers. In one approach a grid cell was identified as containing near-surface permafrost if there was at least one layer in which the soil temperature remained below 0 °C throughout two or more consecutive years when frozen ground conditions were simulated using these models (Guo & Wang, 2013; Lawrence et al., 2012). A requirement for this method is that one whole soil layer (which was perhaps very thick) is frozen during the period, but this does not exactly match the definition of permafrost (Muller, 1947). Surface frost number and surface frost index models have been applied to explore degeneration of permafrost using multiscenario data (Guo & Wang, 2016; Lu et al., 2017), but only the change in permafrost distribution was considered. The active layer thickness (ALT) was neglected owing to the lack of description of the thaw front in this model, even though an increase in ALT is an important indicator of permafrost degradation. Therefore, dynamical representations of FTF depths in land surface and hydrological models are of importance.

A simple method for computing FTF depth is to interpolate soil temperatures (observed or simulated) to obtain a vertical temperature distribution, from which FTF depth can be calculated. However, this method cannot be used to simulate multiple FTFs at the same time when the observed or modeled layer is thick. This direct method for calculating FTF depth also yields numerical oscillations when the soil temperature is close to the freezing or melting point during autumn freezing and spring snowmelt periods (Yi et al., 2006). Some efforts to use the Stefan equation in multilayered systems have been made, especially for engineering applications (Jumikis, 1977; Lunardini, 1981). Fox (1992) incorporated this algorithm into a water balance model. Li and Koike (2003) incorporated a modified Stefan approximation solution (Nelson et al., 1997; Woo et al., 2004) in SIB2, which used surface temperature to calculate single-column FTF depths. Yi et al. (2006) coupled a Stefan algorithm in Community Land Model 3 to explicitly simulate FTF depths. Wang et al. (2010) used a modified Stefan approximation method in a distributed biosphere hydrological model to investigate the role of FTFs. However, these studies did not simulate the permafrost and seasonally frozen ground states or their changes, and their validations of FTF depth simulation were not sufficient.

The objective of this study was to incorporate a new frozen soil parameterization including changes in FTFs into the land model CLM4.5. The simulation results of FTF depths from our model, denoted as CLM4.5_FTF, were validated against multiple sources of observed data. After proving the good performance of the new model in simulating FTFs at both site and region levels, CLM4.5_FTF was applied to several representative stations (D66 is permafrost and Hulugou, Maliantan, Yingke are seasonally frozen ground) for evaluation. Finally, we give the simulated latent heat flux, sensible heat flux, and 10-cm soil temperature deviations determined via the couple model with and without new scheme.

2. Model Development

2.1. CLM4.5

The land surface model used in this study was CLM4.5, developed by the National Center for Atmospheric Research (Oleson et al., 2013). CLM4.5 is the land component of the Community Earth System Model (CESM 1.2.0) (Gent et al., 2011; Hurrell et al., 2013; Li et al., 2013; Zeng et al., 2016a). CLM4.5 includes updates to the photosynthesis, soil biogeochemistry, fire dynamics, cold region hydrology, lake, and biogenic volatile organic compound models from the previous version (Lindsay et al., 2014; Zeng et al., 2017). This land model simulates biogeophysical exchanges of shortwave and longwave radiation, momentum, sensible heat, and latent heat between the land and atmosphere as modified by vegetation and soil; heat transfer in soil and snow; and the hydrologic cycle, including interception of precipitation by vegetation, infiltration, surface and subsurface runoff, soil water redistribution, water table depth, and snow dynamics (Wang & Yang, 2018; Zeng et al., 2016b; Zeng et al., 2018).

Figure 1 shows a schematic diagram of the numerical scheme used to solve for the soil temperature. The soil column is discretized into 15 layers and the depth of soil layer i is

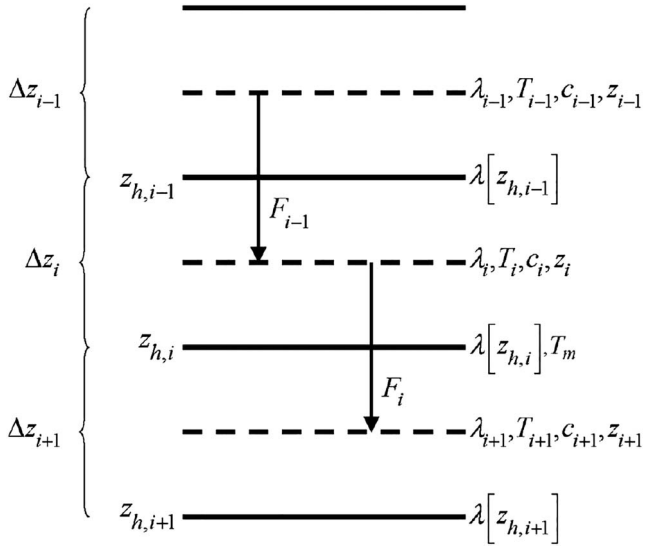

Figure 1. Schematic diagram of the numerical scheme used to solve for the soil temperature. The thermal conductivity λ, specific heat capacity c, and temperature T are defined at the layer node depth z. The thermal conductivity $\lambda[z_h]$ is defined at the interface of two layers z_h. The layer thickness is Δz. The heat fluxes F_{i-1} and F_i are defined as positive upward.

$$z_i = f_s\{\exp[0.5(i-0.5)]-1\} \tag{1}$$

where z_i is the depth of the soil layer i and $f_s = 0.025$ is a scaling factor. The thickness of each layer, Δz_i, is

$$\Delta z_i = \begin{Bmatrix} 0.5(z_1+z_2) & i=1 \\ 0.5(z_{i+1}-z_{i-1}) & i=2,3,\cdots,N_{levgrnd}-1 \\ z_i-z_{i-1} & i=N_{levgrnd} \end{Bmatrix} \tag{2}$$

where $N_{levgrnd} = 15$ is the number of soil layers.

The second law of heat conduction in one-dimensional form is

$$c\frac{\partial T}{\partial t} = \frac{\partial}{\partial z}\left[\lambda\frac{\partial T}{\partial z}\right] \tag{3}$$

where c is the volumetric snow/soil heat capacity ($J\cdot m^{-3}\cdot K^{-1}$) and t is the time (s). T is the soil temperature (K), z is in the vertical direction (m) and is positive downward, and λ is the thermal conductivity ($W\cdot m^{-1}\cdot K^{-1}$).

Equation (3) is solved using the Crank-Nicholson method, which gives us the resulting equation

$$\frac{c_i\Delta z_i}{\Delta t}\left(T_i^{n+1}-T_i^n\right) = h^{n+1} - \alpha\frac{\lambda[z_{h,i}]\left(T_i^n-T_{i+1}^n\right)}{z_{i+1}-z_i} - (1-\alpha)\frac{\lambda[z_{h,i}]\left(T_i^{n+1}-T_{i+1}^{n+1}\right)}{z_{i+1}-z_i} \tag{4}$$

where h (W/m) is the heat flux from the overlying atmosphere and $\alpha = 0.5$ (Figure 1).

Equation (4) is used to calculate the soil and snow temperature for a 15-layer soil column with up to five overlying layers of snow, with the boundary condition that h is the heat flux into the surface snow/soil layer from the overlying atmosphere and there is zero heat flux at the bottom of the soil column.

This temperature profile is calculated first without a phase change, and then readjusted for a phase change. The phase change takes place as

$$\begin{cases} T_i^{n+1} > T_f \text{ and } w_{ice,i} > 0 \; i = snl+1,\cdots,N_{levgrnd} & \text{melting;} \\ T_i^{n+1} < T_f \text{ and } w_{liq,i} > 0 \; i = snl+1,\cdots,0 & \text{freezing} \\ T_i^{n+1} < T_f \text{ and } w_{liq,i} > w_{liq,\max,i} \; i = 1,\cdots,N_{levgrnd} & \text{freezing} \end{cases} \tag{5}$$

where T_i^{n+1} is the soil layer temperature solved using equation (4) with an implicit difference scheme; $w_{ice,i}$ and $w_{liq,i}$ are the mass of ice and liquid water (kg/m^2) in each snow/soil layer, respectively; T_f is the freezing temperature of water (K); snl is the negative of the number of snow layers; and $N_{levgrnd} = 15$ is the number of soil layers. For the freezing process in soil layers, the concept of supercooled soil water described by Niu and Yang (2006) is adopted. Supercooled soil water is the liquid water that coexists with ice over a wide range of temperatures below freezing, and is implemented via an equation for freezing point depression (Fuchs et al., 1978):

$$w_{liq,\max,i} = \Delta z_i\theta_{sat,i}\left[\frac{10^3 L_f\left(T_f-T_i\right)}{gT_i\psi_{sat,i}}\right]^{-1/B_i} \quad T_i < T_f \tag{6}$$

where $w_{liq,max,i}$ is the maximum liquid water in layer i (kg/m^2) when the soil temperature T_i is below the freezing temperature T_f, $\theta_{sat,i}$ is the volumetric water content at saturation, L_f is the latent heat of fusion (J/kg^2), g is the gravitational acceleration (m/s^2), and $\psi_{sat,i}$ and B_i are the soil texture-dependent saturated matrix potential (mm) and the Clapp and Hornberger exponent, respectively (Clapp & Hornberger, 1978).

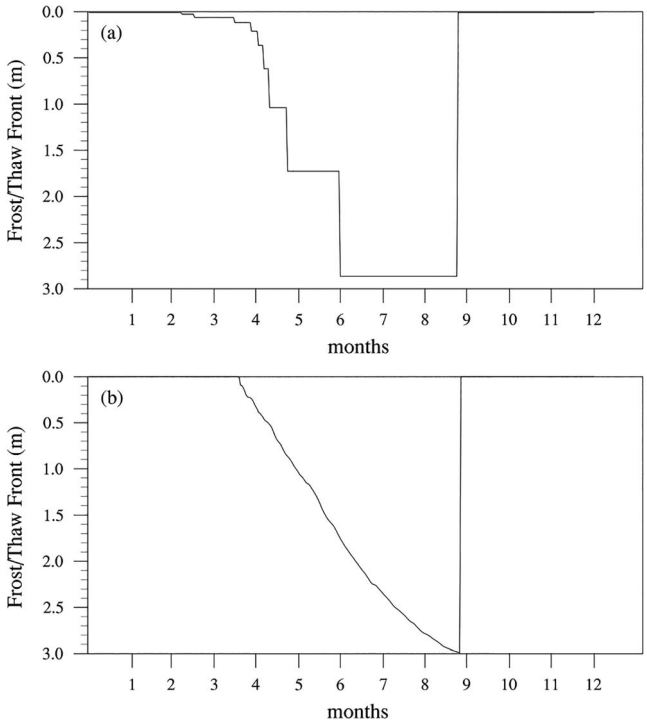

Figure 2. Schematic of a thaw front simulated by (a) CLM4.5 and (b) CLM4.5_FTF.

In the type of frozen soil parameterization used in CLM4.5, the phase transition is modeled using an isothermal approach, with the assumption that the phase transition occurs in the middle of each soil layer. From equation (1), we know that the soil layers will be very thick at depth (e.g., thickness > 1.5 m in 10th soil layer). This parameterization therefore results in a delayed or rapid freezing/thawing process.

2.2. A New Frozen Soil Parameterization Including Frost and Thaw Fronts and Its Implementation in the Community Land Model

The Stefan equation (Jumikis, 1977; Lunardini, 1981; Woo et al., 2004; Zhang & Wu, 2012; Xie et al., 2013; Gao et al., 2016) can be applied to calculate FTFs in a one-directional soil column, for which it is assumed that all of the heat reaching FTFs is used for freezing soil water or for melting soil ice. Little site-specific information is available, so the Stefan solution is frequently used by permafrost scientists to predict frost depth and to simulate heat transfer during water phase transitions in frozen soil.

Figure 2 illustrates the change in the simulated thaw front during the thaw phase. For the original model CLM4.5 (Figure 2a), the front increases from one soil layer to another discontinuously, which is obviously inaccurate. This is because of the assumption that the phase transition occurs in the middle of each soil layer and each soil layer stays in the same freeze–thaw state. In contrast, the energy-based Stefan equation used in this study (Figure 2b) can represent the actual continuous variation of the front.

The Stefan equation can be described in the following form:

$$z_l = \sqrt{\frac{2\lambda \cdot D}{L \cdot \theta}} \tag{7}$$

and

$$D = \left(T - T_f\right)t \tag{8}$$

where z_l ($l = f$ or t) is the FTF depth, λ is the thermal conductivity, D is the freeze/thaw index, t is the freezing or thawing duration, T is the average temperature at the surface, T_f is the freezing/thawing point temperature, L is the volumetric latent heat of fusion, and θ is the volumetric fraction of the soil moisture content.

In this study, the thermal conductivity λ_i ($\mathrm{W \cdot m^{-1} \cdot K^{-1}}$) in soil layer i is calculated using the formulation of Farouki (1981),

$$\begin{aligned} \lambda_i &= \left\{ \begin{array}{ll} K_{e,i}\lambda_{sat,i} + \left(1 - K_{e,i}\right)\lambda_{dry,i} & S_{r,i} > 1\times10^{-7} \\ d_{dry,i} & S_{r,i} \le 1\times10^{-7} \end{array} \right\} \quad i = 1, \cdots, N_{levsoi} \\ \lambda_i &= \lambda_{bedrock} \qquad\qquad\qquad\qquad\qquad\qquad\quad i = N_{levsoi} + 1, \cdots, N_{levgrnd} \end{aligned} \tag{9}$$

where $\lambda_{sat,I}$ is the saturated thermal conductivity, $\lambda_{dry,I}$ is the dry thermal conductivity, $K_{e,i}$ is the Kersten number, $S_{r,i}$ is the wetness of the soil with respect to saturation, and $\lambda_{bedrock}$ is the thermal conductivity assumed for the deep ground layers. The saturated thermal conductivity $\lambda_{sat,I}$ depends on the thermal conductivities of the soil, liquid water, and ice constituents

$$\lambda_{sat} = \lambda_s^{1-\theta_{sat}} \lambda_{liq}^{\frac{\theta_{liq}}{\theta_{liq}+\theta_{ice}}\theta_{sat}} \lambda_{ice}^{\theta_{sat}\left(1-\frac{\theta_{liq}}{\theta_{liq}+\theta_{ice}}\right)} \tag{10}$$

where λ_{liq} and λ_{ice} are the thermal conductivities of liquid water and ice, respectively. The thermal conductivity of soil solids $\lambda_{s,i}$ varies depending on the sand, clay and organic matter content

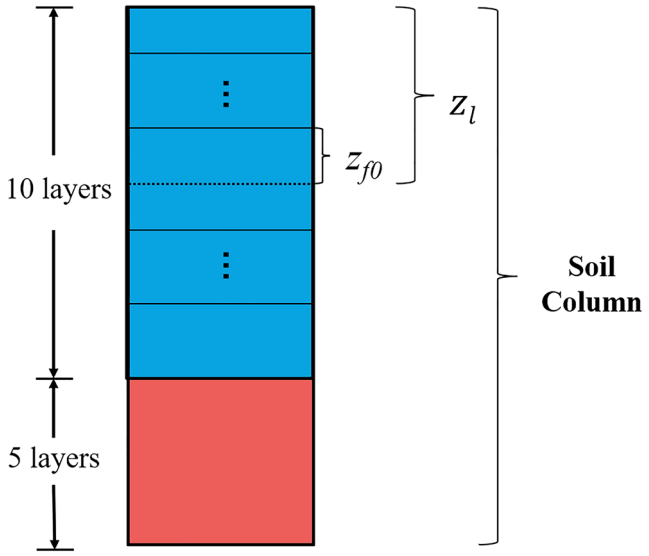

Figure 3. Schematic diagram of a freeze or thaw front in a vertical column. The top 10 layers are hydrologically active soil layers and the bottom five layers are dry bedrock layers.

$$\lambda_{s,i} = \left(1-f_{om,i}\right)\lambda_{s,\min,i} + f_{om,i}\lambda_{s,om} \tag{11}$$

where $f_{om,i}$ is the soil layer organic matter fraction.

Because each soil layer has a different thermal conductivity and soil moisture content in CLM4.5 (Figure 1), equation (7) cannot be used directly to solve for the FTF depth. To address this, we define N_i as the requirement of the freeze/thaw index for the frost/thaw front to pass from z_{i-1} to z_i (Gao et al., 2016; Xie et al., 2018), then

$$\begin{aligned} N_1 &= (L\cdot\theta_1\cdot z_1)\left(\frac{R_1}{2}\right) \\ N_2 &= (L\cdot\theta_2\cdot z_2)\left(R_1+\frac{R_2}{2}\right) \\ &\cdots \\ N_i &= (L\cdot\theta_i\cdot z_i)\left(\sum_{n=1}^{i-1} R_n + \frac{R_i}{2}\right) \end{aligned} \tag{12}$$

where the thermal resistance in layer i is $R_i = \Delta z_i/\lambda_i$. When the freeze/thaw index $D \geq \sum_{n=1}^{i-1} N_n$ and $D < \sum_{n=1}^{i} N_n$, we can obtain z_{f0} (shown in Figure 3) as follow:

$$z_{f0} = -\lambda_i \sum_{n=1}^{i-1} R_n + \left\{\lambda_i^2\left[\sum_{n=1}^{i-1} R_n\right]^2 + \left[2\lambda_i\left(D - \sum_{n=1}^{i-1} N_n\right)/(L\cdot\theta_i)\right]\right\}^{1/2} \tag{13}$$

where the FTF depth is

$$z_l = z_{i-1} + z_{f0} \tag{14}$$

Using this method, we can calculate the FTF depths z_l ($l = f$ or t) at time step $n+1$ using the values for z_l ($l = f$ or t), D, and N_i at time step n.

In the simulation process, each complete freeze–thaw cycle is divided into two phases: freezing and thawing. To avoid the potential impact of random surface temperature on the movement from one phase to the other, we assume that if the average daily surface temperature remains below 0 °C for five consecutive days, the first of these days is considered as the start of the freezing phase (Guo & Wang, 2013). This phase continues until the daily surface temperature is >0 °C for five consecutive days. The beginning and end of the thawing phase are defined analogously.

In this study, FTF depths are calculated as daily variables, while the default time step of CLM4.5 is 1,800 s. This is because the Stefan solution behaves better in accounting for daily but not diurnal penetration of FTFs, and our focus is on changes in FTFs in one year or several decades with climate change. Thus, T is the daily average ground temperature and t is 86,400 s in equation (8). The first soil layer temperature (from 0 to 0.0175 m) was used as the ground temperature in the calculations instead of the air temperature, because this manipulation can remove the influences of surface vegetation and snow cover. We define the maximum FTF depth as the bottom edge of the 10th soil layer (3.8 m) in this study. This is because the top 10 layers for the 15-layer soil column are hydrologically active, while the next 5 layers are dry bedrock layers. We did not consider the freeze–thaw processes in these bedrock layers because of the zero volumetric soil water content.

Depending on the frozen state and the length of its retention time, frozen soil can be categorized as permafrost or seasonally frozen ground. Permafrost is defined as a region where the soil temperature remains below 0 °C for a period of two or more consecutive years (Muller, 1947). Frozen soil regions that do not meet this definition are classed as seasonally frozen ground. Permafrost is mainly distributed in high-latitude and high-altitude areas where the annual mean air temperature is <0 °C. The soil thaws in the near surface in summer, and the thawed soil then refreezes until the whole soil column is completely frozen in winter. By contrast, seasonally frozen ground is distributed in areas where the annual average air temperature is >0 °C. The soil column completely thaws in the summer in these regions.

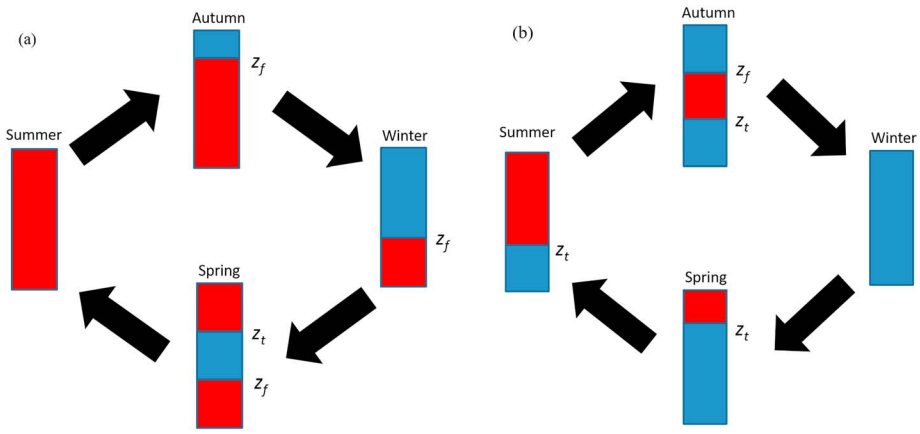

Figure 4. Schematic diagram of the soil freezing and thawing cycle in (a) seasonally frozen ground and (b) permafrost. Red denotes liquid water and blue denotes ice in the soil column.

The soil freeze–thaw cycle is completely different in permafrost and in seasonally frozen ground. The frost front depth is greater than the thaw front in seasonally frozen ground, whereas the opposite is the case for permafrost, as shown in Figure 4. Therefore, we need to distinguish the different types of frozen soil when coupling the algorithm in section 2.2 with CLM4.5. The initial values for the frost front z_f, z_f^*, and the thaw front z_t are all 0 m. For time step $n+1$, the calculation process is as follows using the values obtained in the nth time step:

1. In the thawing phase, if the frost front satisfies $z_f^n>0$, then this proves that the soil was frozen in the previous freezing phase and this region can be classified as frozen. The frost front remains unchanged and we need to calculate the thaw front under this condition. If the thaw front z_t in the nth time step satisfies $z_{h,i-1}\le z_t^n<z_{h,i}$, where $z_{h,i}$ is the depth at the layer interface, then

$$D=\left[\left(z_t^n-z_{h,i-1}+\lambda_i\sum_{n=1}^{i-1}R_n\right)-\lambda_i^2\left(\sum_{n=1}^{i-1}R_n\right)^2\right]\frac{L\cdot\theta_i}{2\lambda_i}+\sum_{n=1}^{i-1}N_n+(T-T_f)t \tag{15}$$

Combining equations (12), (13), (14), and (15), we can obtain z_t in time step $n+1$. If $z_f^n>z_t^n$ and $z_f^{n+1}<z_t^{n+1}$, this means that the column is completely melted. We set $z_f^{n+1}=0$ and $z_t^{n+1}=0$.

2. In the thawing phase, if$z_f^n=0$, this proves that the soil did not freeze in the previous freezing phase and this region can be classified as unfrozen or else the frozen soil melted completely. We set $z_f^{n+1}=0$ and $z_t^{n+1}=0$.
3. In the freezing phase, if the thaw front satisfies $z_t^n=0$, then the thaw front remains unchanged and we need to calculate the frost front. If z_f in the nth time step satisfies$z_{h,i-1}\le z_f^n<z_{h,i}$, then

$$D=\left[\left(z_f^n-z_{h,i-1}+\lambda_i\sum_{n=1}^{i-1}R_n\right)-\lambda_i^2\left(\sum_{n=1}^{i-1}R_n\right)^2\right]\frac{L\cdot\theta_i}{2\lambda_i}+\sum_{n=1}^{i-1}N_n+(T_f-T)t \tag{16}$$

Combining equations (12), (13), (14), and (16), we can obtain z_f in time step $n+1$.

4. In the freezing phase, if$z_t^n>0$, this means that the soil column did not thaw completely in the previous thawing phase and this region can be classified as permafrost. Then the thaw front z_t and the original frost front z_f remain unchanged: $z_t^{n+1}=z_t^n$ and $z_f^{n+1}=z_f^n$. A new frost front z_f^* is then calculated under this condition. If $z_{h,i-1}\le z_f^{*n}<z_{h,i}$, then

$$D=\left[\left(z_f^{*n}-z_{h,i-1}+\lambda_i\sum_{n=1}^{i-1}R_n\right)-\lambda_i^2\left(\sum_{n=1}^{i-1}R_n\right)^2\right]\frac{L\cdot\theta_i}{2\lambda_i}+\sum_{n=1}^{i-1}N_n+(T_f-T)t \tag{17}$$

Combining equations (12), (13), (14), and (17), we can obtain z_f^* in time step $n+1$. If $z_f^{*n}>z_t^n$ and $z_f^{*n+1}<z_t^{n+1}$, this means that the column is completely frozen. Then we set $z_f^{*n+1}=0$ and $z_t^{n+1}=0$.

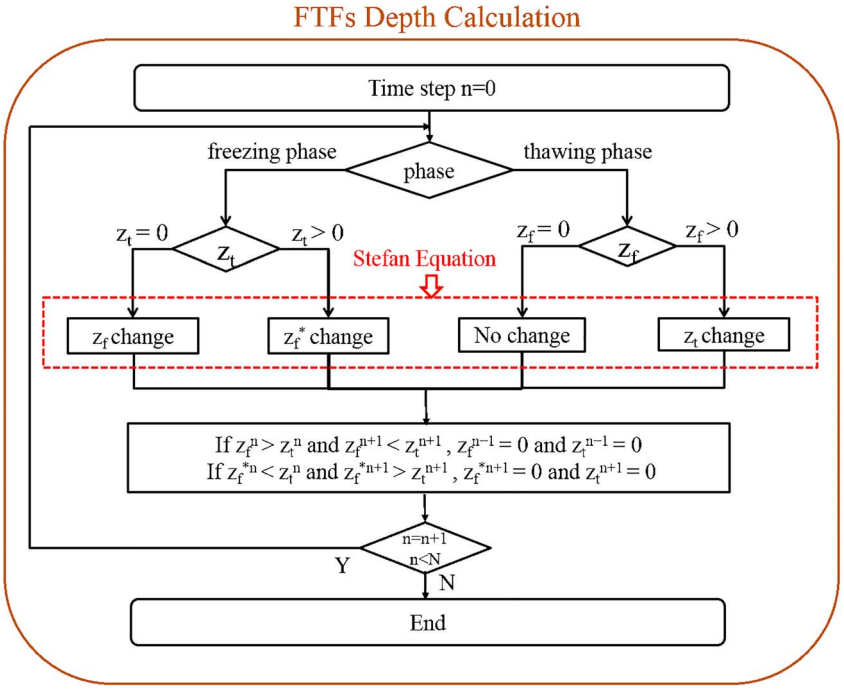

Figure 5. Schematic diagram of numerical simulation of FTFs in our CLM4.5_FTF model.

Figure 5 shows a schematic diagram of numerical simulation of FTFs in our CLM4.5_FTF model. The frozen ground region is considered as permafrost if the soil column did not melt completely after the thawing phase ($z_f > z_t$ for the whole phase), and the condition whereby more than one whole soil layer must be frozen throughout two or more consecutive years is not needed. Then permafrost and seasonally frozen ground can be distinguished more precisely.

After determining the position of the frost or thaw front, we estimate the soil temperature profile to improve the frozen soil parameterization (Figure 6). The iteration is included in the following steps:

I. Treat the position of FTF as a new layer node in equation (1), and then calculate the thickness of each layer Δz_i using equation (2). The parameters, including the soil heat capacity and conductivity based on the new soil layers, also need to be updated.
II. Considering T_f as the new layer node temperature, we can calculate the soil temperature T_i ($l = f$ or t) at time step $n + 1$ using the values of T_i and the boundary conditions at time step n according to equation (4).
III. Return the new node temperature at time step $n + 1$ to the original soil layers. Determine if a phase change has occurred based on equations (5) and (6) (Clapp & Hornberger, 1978), then update the soil temperature and water content.
IV. Calculate the FTFs in the next time step according to equations (12)–(17).
V. Return to repeat steps (I) to (IV).

3. Data and Experimental Design

3.1. Data

We collected data from multiple sources to validate the performance of our new CLM4.5_FTF model. Daily FTF data from 1 September 1997 to 22 September 1998 for the D66 station located in the northern part of the Tibetan Plateau were linearly interpolated from observed soil temperature data in 10 layers (4, 20, 40, 60, 80, 100, 130, 160, 200, and 250 cm) obtained at hourly intervals from GAME-Tibet (the GEWEX Asian Monsoon Experiment on the Tibetan Plateau; Wang et al., 2014). Daily FTF data (from 2011 to 2012) for the Hulugou station and daily data for Maliantan and Yingke station (from 2008 to 2009) in the Heihe River basin were obtained from the Cold and Arid Regions Science Data Center at Lanzhou (Chen et al., 2014). The

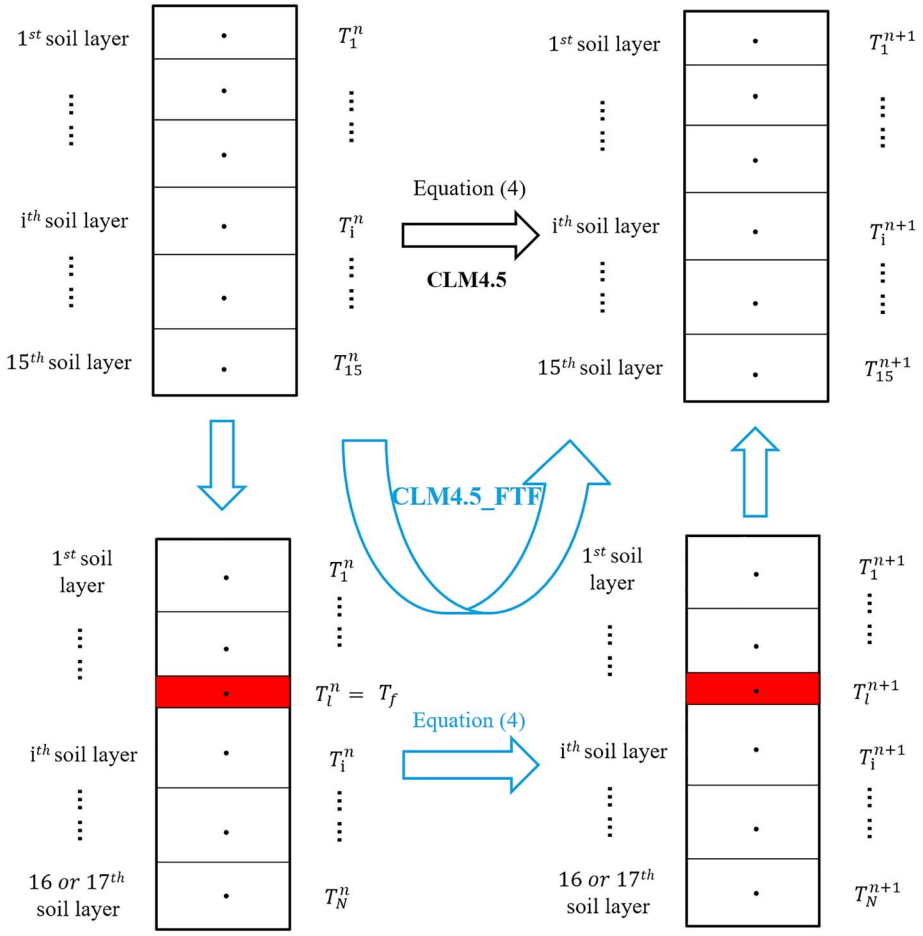

Figure 6. Schematic diagram of the frozen soil parameterization in CLM4.5 and CLM4.5_FTF.

Circumpolar Active Layer Monitoring (CALM) program, established in the 1990s, observes the long-term response of the active layer and near-surface permafrost to changes and variations in climate (https://www2.gwu.edu/~calm/data/data-links.html). We selected ALT data from 19 sites with a long and continuous observation period from the CALM database. These observations were used for comparison with the maximum simulated thaw front in permafrost, which is considered as the ALT, according to our model. Details for the observation sites are listed in Table 1. The frozen ground map of China used to validate the simulated frozen ground distributions was developed by Li et al. (2008) and is thought to provide a reasonable distribution pattern for permafrost and seasonally frozen ground in China. The International Permafrost Association (IPA) map (Brown et al., 1998), comprising observations of permafrost distribution, was used to validate our permafrost simulations for the Northern Hemisphere. The data are archived at http://nsidc.org/data/docs/fgdc/ggd318_map_circumarctic/index.html.

CRUNCEP (Piao et al., 2012) is a 110-year (1901–2010) data set that provides standard forcing for CLM4.5. It is a combination of two existing data sets: CRU TS3.2 0.5° × 0.5° monthly data covering the period 1901–2002 (Mitchell & Jones, 2005) and National Centers for Environmental Prediction (NCEP) reanalysis 2.5° × 2.5° 6-hourly data covering the period 1948–2010 (Kalnay et al., 1996). However, CRUNCEP does not cover the period of observations for the Hulugou station, so we need another forcing data set to validate simulated FTFs for the Hulugou site. To this end, we obtained the atmosphere forcing data set (ITP data set) for 2011–2012 from the Data Assimilation and Modeling Center for Tibetan Multi-spheres, Institute of Tibetan Plateau Research, Chinese Academy of Science (Yang et al., 2010; Zeng et al., 2017).

Table 1
Information for Observation Sites Used in This Study

Site	Latitude	Longitude	Location	Period	Types of Data	Types of Frozen Ground	Case
D66	35°31′N	93°47′E	Tibetan Plateau	September 1997 to September 1998	Daily FTFs	Permafrost	
Hulugou	38°16′N	99°53′E	Heihe River Basin, China	2011–2012	Daily FTFs	Seasonally frozen ground	
Maliantan	38°32′N	100°17′E	Heihe River Basin, China	2008–2009	Daily	Seasonally frozen ground	
Yingke	38°51′N	100°25′E	Heihe River Basin, China	2008–2009	Daily	Seasonally frozen ground	
West Dock	70°22′N	148°34′W	Alaska North Slope	1996–2010	ALT	Permafrost	1
Deadhorse	70°10′N	148°28′W					
Betty Pingo	70°17′N	148°52′W					
Franklin Bluff	69°41′N	148°43′W	Alaska North Slope	1996–2010	ALT	Permafrost	2
Happy Valley	69°06′N	148°30′W					
Lupine Hill	69°08′N	148°36′W					
Lousy Point	69°13′N	134°17′W	Canada	1992–2010	ALT	Permafrost	3
Reindeer Depot	68°41′N	134°8′W					
Rengleng River	67°48′N	134°8′W	Canada	1992–2010	ALT	Permafrost	4
Ochre River	63°28′N	123°42′W	Canada	1993–2010	ALT	Permafrost	5
Willowlake River	62°42′N	123°3′W					
Ayach-Yakha, Vorkuta	67°35′N	64°11′E	Russian European north	1998–2010	ALT	Permafrost	6
Talnik	67°20′N	63°44′E					
Nadym	65°20′N	72°55′E	West Siberia	1997–2010	ALT	Permafrost	7
Marre Sale	69°43′N	66°45′E	West Siberia	1995–2010	ALT	Permafrost	8
Akhmelo channel	68°49′N	161°00′E	North East Siberia	1996–2010	ALT	Permafrost	9
Mount Rodinka	68°45′N	161°30′E					
Cape Rogozhny	64°47′N	176°58′E	Chukotka	1994–2010	ALT	Permafrost	10
Zackenberg	74°28′N	20°30′W	Denmark (Greenland)	1996–2010	ALT	Permafrost	11

3.2. Experimental Design

First, we tested the sensitivity of the freezing and thaw phase definitions. Then, we used CLM4.5_FTF model to simulate changes in FTFs for the D66 station, which is underlain by permafrost, from 1 September 1997 to 22 September 1998 using CRUNCEP atmosphere forcing data. We also ran the simulation for the Hulugou, Maliantan, and Yingke sites using ITP atmosphere forcing data. The observations at 19 sites from the CALM database were divided into 11 cases according to their location to validate the active layer depth simulated using our model (Table 1). The sites in all cases were on the same 1° × 1° grid. Then the average of observed ALT values for each site was used for comparison with the model simulation for that site to reduce the uncertainty of the observations.

Simulations for regions in China were performed from 1980 to 2010 using CRUNCEP atmosphere forcing data. The model domain was 15°–55°N and 70°–140°E and the spatial resolution was 0.5° × 0.5° in longitude and latitude. Global simulation was also performed from 1980 to 2010 using CRUNCEP forcing data at a spatial resolution of 0.9° × 1.25° in longitude and latitude. The site and regional simulations were both run for 100 years to obtain a quasi-steady state before the formal simulation, and all experiments were taken as "offline" simulation.

To investigate the effects of the frozen soil parameterization considering changes in FTF depths, two simulation scenarios were established. The first simulation used the original version of CLM4.5, while the second used the new CLM4.5_FTF model. The effects were examined by mapping the differences in soil temperature, soil moisture, the dates for freeze start and end, and freeze duration between the two simulations for the D66, Hulugou, Maliantan, and Yingke sites.

Two sets of numerical experiments were conducted using the original CESM1.2.0 (referred to as CTL) and CESM1.2.0_FTF (referred to as EXP) coupled with the new frozen soil parameterization to investigate the impacts of the new scheme in the coupled model. The simulations were conducted for a 44-year duration from 1970 to 2013 with horizontal spacing of 0.9° × 1.25°. The EXP-minus-CTL difference can be seen as the impact of new scheme in these experiments.

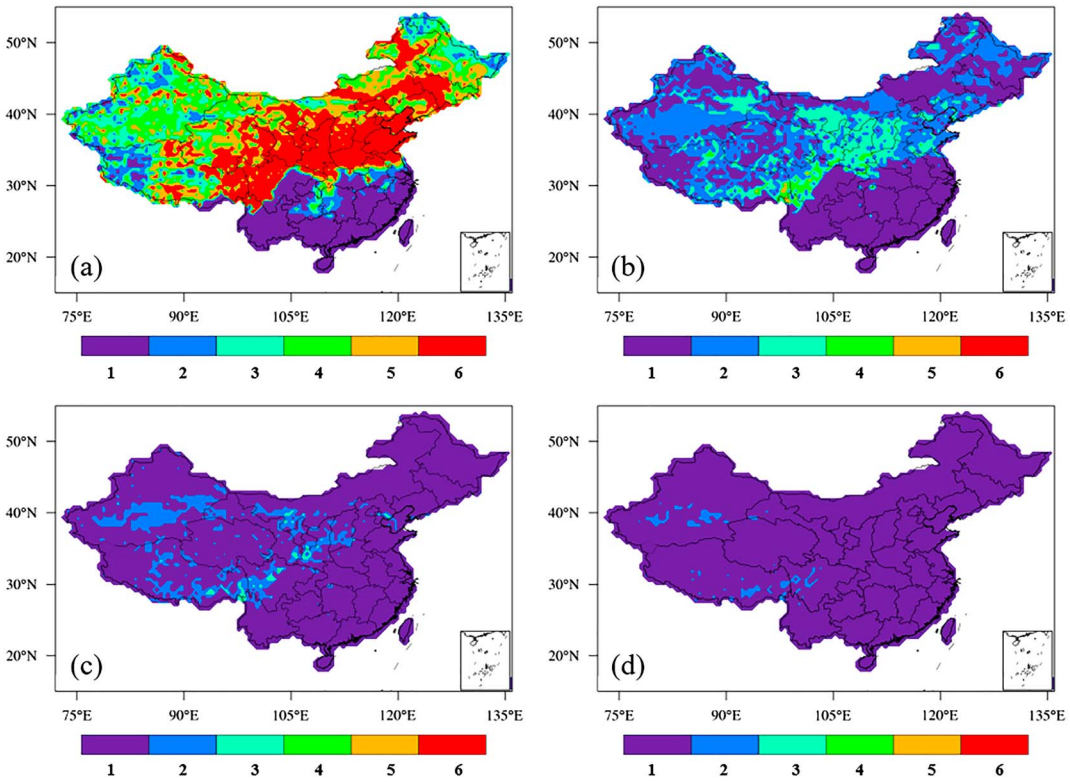

Figure 7. The number of freezing and thawing phases that will occur in one year if we select (a) one day, (b) three days, (c) four days, and (d) five days as the start of the freezing or thawing phase.

4. Model Validation

4.1. Sensitivity Test

In this study, we assumed that if the average daily surface temperature remains below 0 °C for five consecutive days, the first of these days is considered as the start of the freezing phase. This phase continues until the daily surface temperature is >0 °C for five consecutive days. The beginning and end of the thawing phase are defined analogously.

Figure 7 shows the number of freezing and thawing phases that will occur in one year if we select different days as the start of the freezing or thawing phase. If one day is chosen, there will be more than six freezing/thawing phases in the same year because of the random surface temperatures that occur during autumn freezing and spring snowmelt periods. With an increase of the chosen day number, the potential impact of random surface temperatures decreases. When the number is chosen as five, the year is almost divided to one freezing and thawing phase as we hoped.

4.2. Daily FTF Depths

Figure 8a compares simulated and observed daily FTF depths at the D66 station from 1 September 1997 to 22 September 1998. The results show that our new model generally gives a realistic year-long FTF depth profile, with CCs for the frost front and thaw front of 0.98 and 0.98, respectively, and corresponding RMSEs of 0.35 and 0.33 m. The D66 site on the Tibetan Plateau is underlain by permafrost (Table 1). Thus, the deeper frost front z_f is not the actual value but a sign of permafrost. Persistence of z_f for the whole freezing and thawing process means that the soil column does not melt completely. In this case we use a new variable z_f^* to represent the frost front in the active layer in permafrost. The maximum frost front depth observed is 2.5 m because of the limitations of the observation conditions, so the whole freezing and thawing process cannot be revealed by the observed data. The simulated FTFs indicate that the soil column was completely frozen before the thawing phase began. In the thawing phase, the depth of the thaw front below the surface

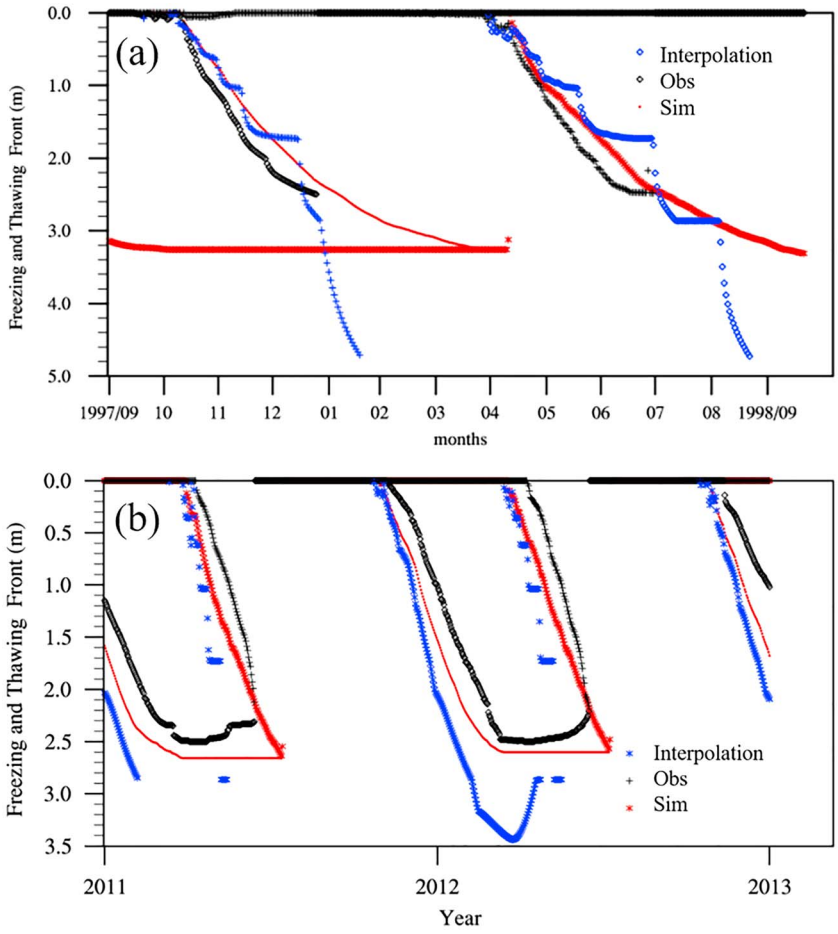

Figure 8. Observed and simulated daily FTFs for (a) permafrost at site D66 and (b) the Hulugou site according to our CLM4.5_FTF model. The horizontal axis ranges from (a) 1 September 1997 to 22 September 1998 and (b) 2011 to 2012.

increased until the next period. Then the frost front (z_f^*) became deeper until it reached the location of the thaw front in this phase. The soil column completely froze again and one cycle was completed.

The daily observed and simulated FTF depths at the Hulugou site from 2011 to 2012 are shown in Figure 8b. The observed values agree well with the simulated data, with correlation coefficients (CCs) for the frost front and thaw front of 0.82 and 0.77, respectively, and corresponding root mean squared errors (RMSEs) of 0.68 and 0.77 m. The Hulugou site in the Heihe River basin is underlain by seasonally frozen ground (Table 1). Before the freezing phase begins in winter, the soil column has thawed completely. Then the frost front moves from the surface to deep soil until the thawing phase. When the thawing phase begins, the depth of the thaw front below the surface increases and reaches the location of the frost front in this period. Then the soil column melts completely and one cycle ends.

The FTF depth is neglected in the original CLM4.5. Then, we interpolated the soil temperatures to find the 0 °C isotherm which is considered as the corresponding FTF depth, and it is shown as the blue lines in Figure 8. This direct method yields numerical oscillations when the soil temperature is close to the freezing or melting points. The results show that the new model gives a more realistic simulation than this method.

4.3. ALT

In section 2.3 we defined the maximum simulated thaw front depth in permafrost as the simulated ALT. Comparisons of observations and model calculations for 11 cases in different Northern Hemisphere areas (Table 1) are shown in Figure 9. To generate these scatterplots, we choose 19 CALM sites and calculated

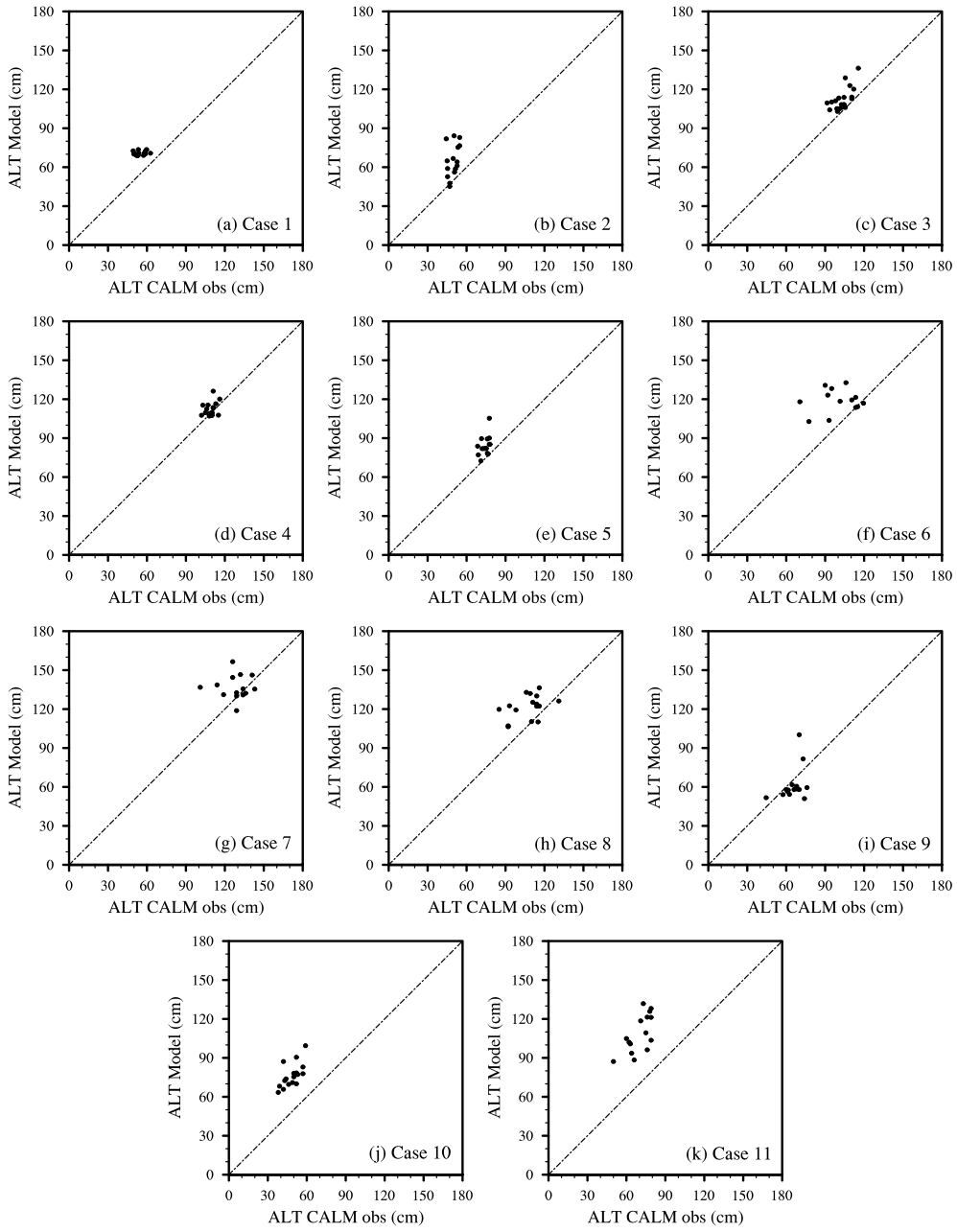

Figure 9. Scatterplots of ALT for CALM sites according to our CLM4.5_FTF model. Table 1 lists further information for the sites and cases.

the average of ALT value if more than one site was located in the same grid cell in the model. Then values for the grid cells were plotted against the climatological ALT values for the CALM sites corresponding to the grid cells. However, there was a scale mismatch for the comparison of observation and simulation data: observed ALT data from CALM sites are for a particular location, while the model-simulated ALT values represent the mean ALT for a grid cell. Furthermore, the ALT observations change substantially over a short distance. Despite these issues, the results show that the simulated ALT data are in general agreement with CALM observations. We assumed that all of the heat reaching the thaw front was used for melting the soil ice and ignored the soil sensible heat when the soil became warmer. Thus, the simulated ALT values are slightly greater than the observed data.

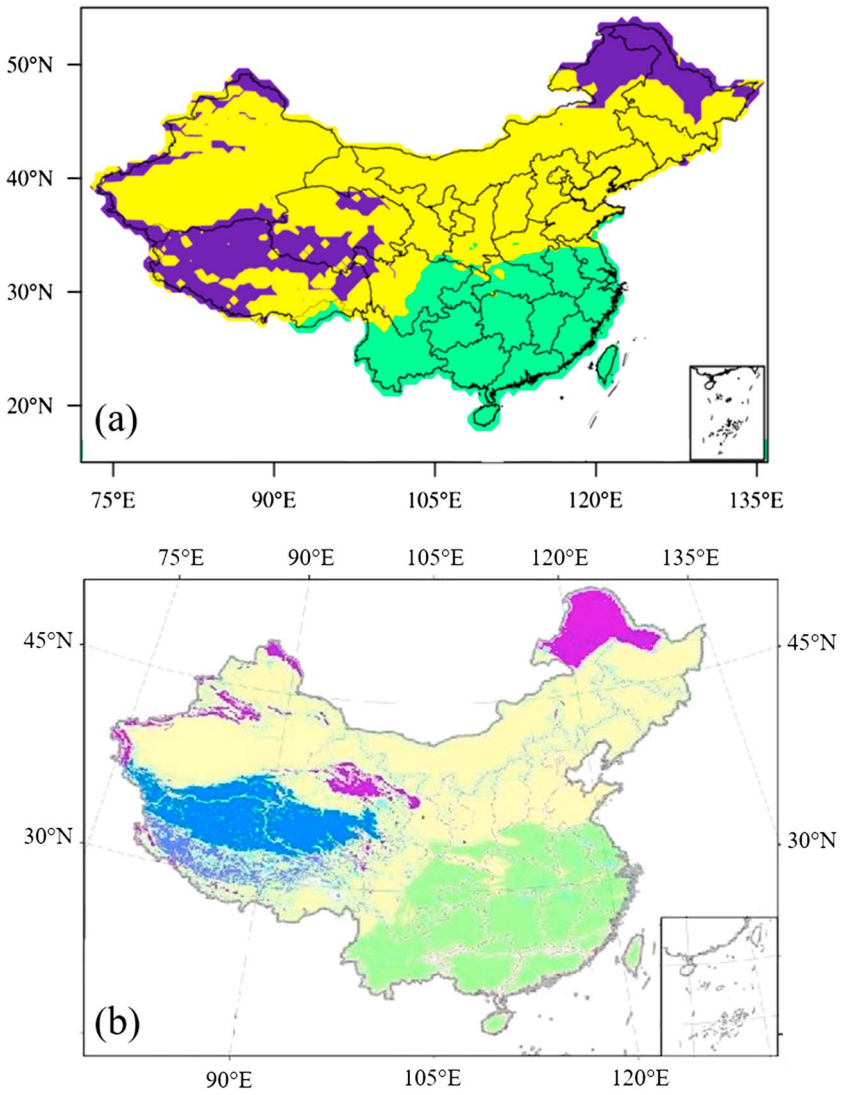

Figure 10. (a) Simulated distribution of frozen ground in China according to our CLM4.5_FTF model. (b) Observed distribution from the frozen ground map of China. The blue and purple region represents permafrost, the yellow region is seasonally frozen ground, and the green region is short-time frozen or nonfrozen ground.

4.4. Frozen Ground Distribution

Figure 10 shows simulated and observed distributions of frozen ground in China. Most of the permafrost in China according to our simulation is on the Tibetan Plateau, in northeastern China, in Tianshan, the Altai Mountains of Xinjiang Province, and other mountainous areas, as shown in Figure 10a. According to the frozen soil map of China, which is a map of the glaciers, frozen ground, and desert in China (Wang, 2006), permafrost and seasonally frozen ground occupy 72% of the land territory in China. The permafrost area in China is approximately 1.72×10^6 km^2 and the seasonally frozen ground area is approximately 5.21×10^6 km^2, as shown in Figure 10b (Li et al., 2008). The simulated permafrost and seasonally frozen ground distributions are very similar to the frozen soil map of China. However, the simulation resulted in a slightly greater permafrost area in northeastern China compared to the map data. This difference could be caused by possible inaccuracies in the forcing data.

Figure 11 shows the observed and simulated distributions of permafrost in the Northern Hemisphere. Permafrost is mostly distributed at high latitudes near the Arctic Circle and at intermediate latitudes in

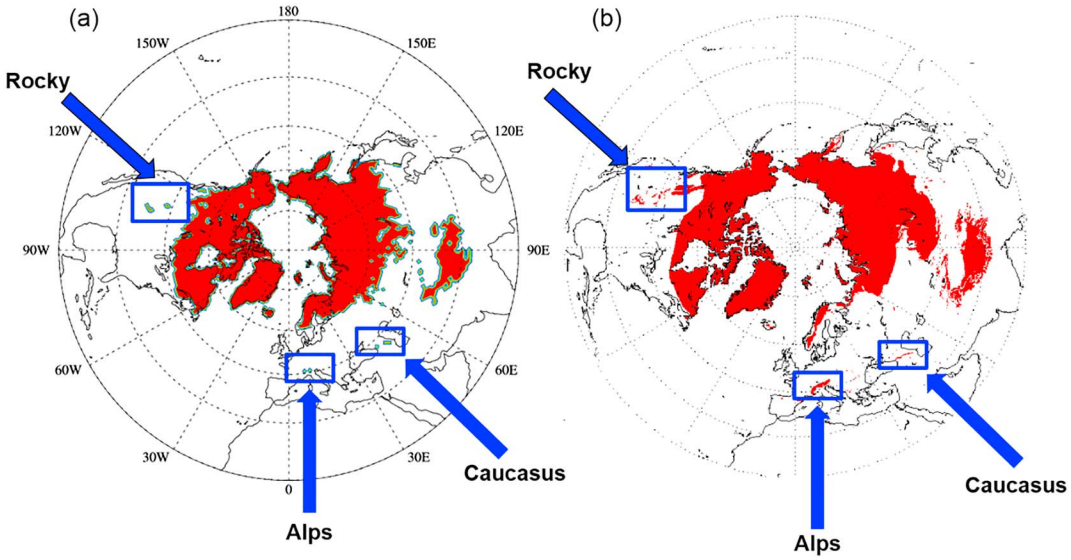

Figure 11. (a) Simulated and (b) observed distribution of permafrost in the Northern Hemisphere. The observed distribution is from the International Permafrost Association map.

high-altitude areas such as the Qinghai-Tibet Plateau, the Rocky Mountains, the Greater Caucasus Mountains, and the Alps. Although the simulated spatial resolution is not high (0.9° × 1.25°), our CLM4.5_FTF model can accurately simulate permafrost distribution in the Northern Hemisphere as verified from the IPA map. The model produced an ensemble mean permafrost area of 14.97×10^6 km^2, which compares reasonably well with the area of 15.24×10^6 km^2 in the observation.

5. Evaluation of the New Frozen Soil Parameterization

The above validation confirms that CLM4.5_FTF performs well in simulating FTF depths at both site and region levels. We then isolated the effects of the frozen soil parameterization considering FTF changes. The most important element impacted by this parameterization is the soil temperature. Then the changes in soil temperature profiles affect soil moisture through the phase change process.

Figures 12a–12d show the daily soil temperature at 6, 20, 60, and 160 cm at the D66 station (permafrost) from 1 September 1997 to 22 September 1998, simulated using the original CLM4.5 and our new CLM4.5_FTF. Although both soil temperature simulations are close to the observed data, the results show that the new model gives a more realistic year-long soil temperature profile than the original model. For the soil temperature at 6, 20, 60, and 160 cm, the RMSE is 2.29, 1.24, 0.74, and 0.81 for CLM4.5_FTF, and 2.33, 1.26, 0.77, and 0.88 for the CLM4.5 results, respectively (Table 2). The simulations by the two models in shallow soil are basically the same, but the improvement using CLM4.5_FTF is better in the lower levels than in the upper level. This is because when the model considers the change in FTFs, the soil temperature profile can be estimated according to the position of the FTFs. At lower depths, the soil layer is thicker and the effect of the FTF position is more pronounced.

The simulation results for soil moisture using CLM4.5_FTF are compared with observations and the CLM4.5 results in Figures 12e–12h. The simulated results are slightly greater than the observed data, which is primarily attributed to possible inaccuracies in the soil organic matter content and the atmospheric forcing data. However, it is evident that in general the model estimates the freezing duration with acceptable accuracy. The CLM4.5 results represent a rapid freezing process compared to the observations, while the new frozen soil parameterization significantly improved the freezing process estimation, especially in the deeper levels. First of September 1997 is defined as the first day, and detailed information on the date of the freeze start and end and the freeze duration is presented in Table 3.

We carried out similar sets of experiments for the Hulugou, Maliantan, and Yingke sites, which are covered by seasonally frozen ground, and the conclusions are similar. The CLM4.5_FTF model with the new frozen

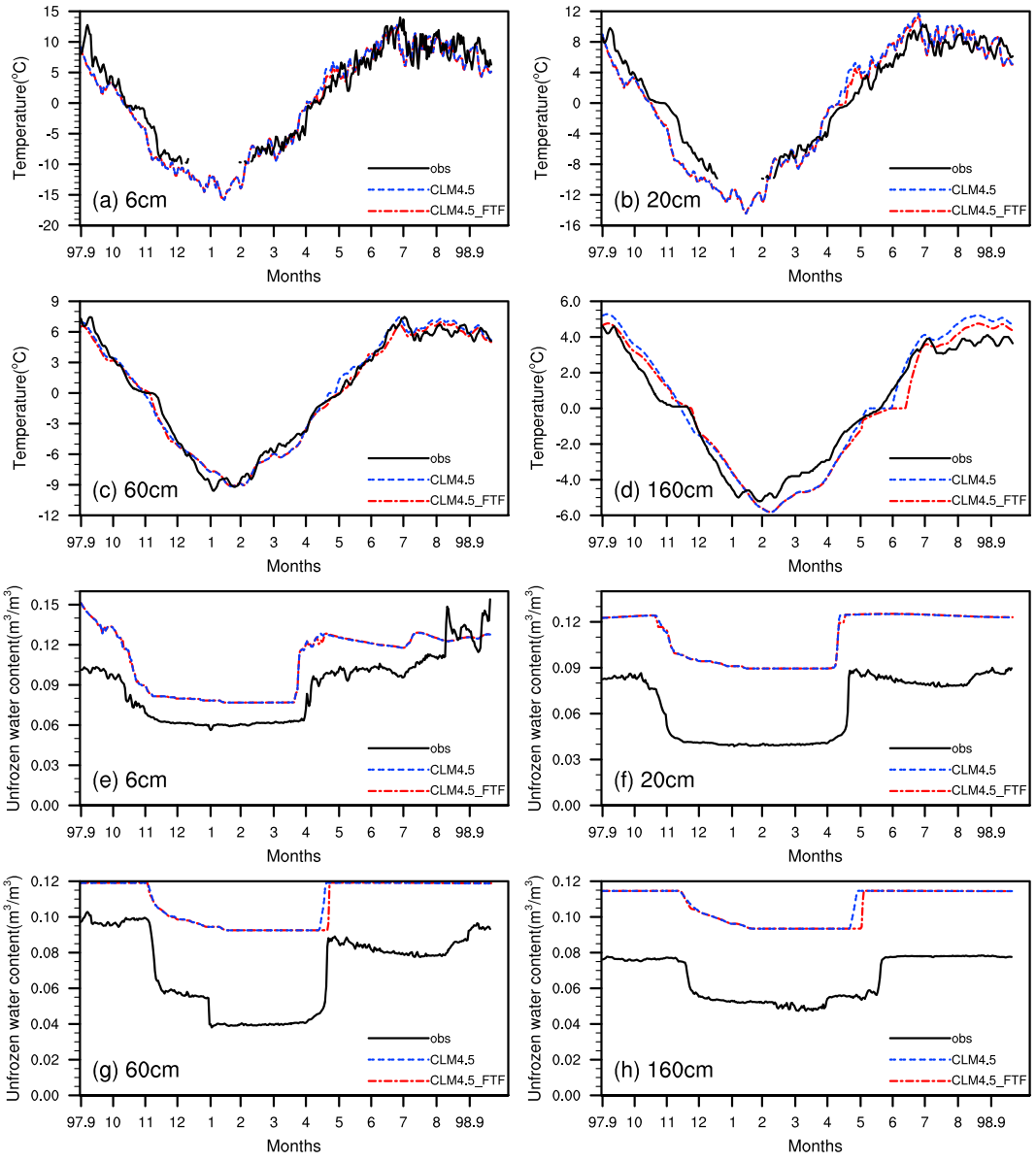

Figure 12. Observed and simulated soil temperature and soil moisture according to CLM4.5_FTF and CLM4.5 for different soil layers at the D66 site.

Table 2
CCs and RMSEs Between Simulations of Soil Temperature With CLM4.5 and CLM4.5_FTF and Observations in Different Soil Layers

		6/20 cm		20/40 cm		60/80 cm		160/120 cm	
Site	Model	CC	RMSE	CC	RMSE	CC	RMSE	CC	RMSE
D66	CLM4.5	0.91	2.33	0.96	1.26	0.97	0.77	0.98	0.88
	CLM4.5_FTF	0.92	2.29	0.96	1.24	0.97	0.74	0.97	0.81
Hulugou	CLM4.5	0.95	3.59	0.92	4.33	0.97	1.75	0.95	1.59
	CLM4.5_FTF	0.96	2.97	0.95	3.43	0.98	1.43	0.97	0.79
Maliantan	CLM4.5	0.95	3.81	0.97	2.40	0.94	2.84	0.94	2.38
	CLM4.5_FTF	0.96	3.11	0.97	1.89	0.96	2.00	0.94	1.76
Yingke	CLM4.5	0.94	7.13	0.91	7.11	0.93	6.40	0.91	6.84
	CLM4.5_FTF	0.94	7.18	0.93	7.16	0.92	6.99	0.93	7.07

Table 3
Freeze/Thaw Start Date, End Date, and Duration Simulated by CLM4.5_FTF and CLM4.5 Are Compared With the Observations at the D66 Site (First Day Is 1 September 1997) and Hulugou Site (First Day Is 1 January 2011)

		CLM4.5_FTF (day)			CLM4.5 (day)			Observation (day)		
Sites	Depth	Start	End	Duration	Start	End	Duration	Start	End	Duration
D66	20 cm	41	211	170	40	211	171	42	217	175
	60 cm	46	226	180	45	221	176	58	231	173
	100 cm	53	231	178	50	227	177	67	243	176
	160 cm	65	243	178	59	238	179	85	260	175
Hulugou	20 cm	102	319	217	94	315	221	104	327	223
	80 cm	123	352	229	114	347	233	128	358	230
	120 cm	144	/	/	128	/	/	139	/	/

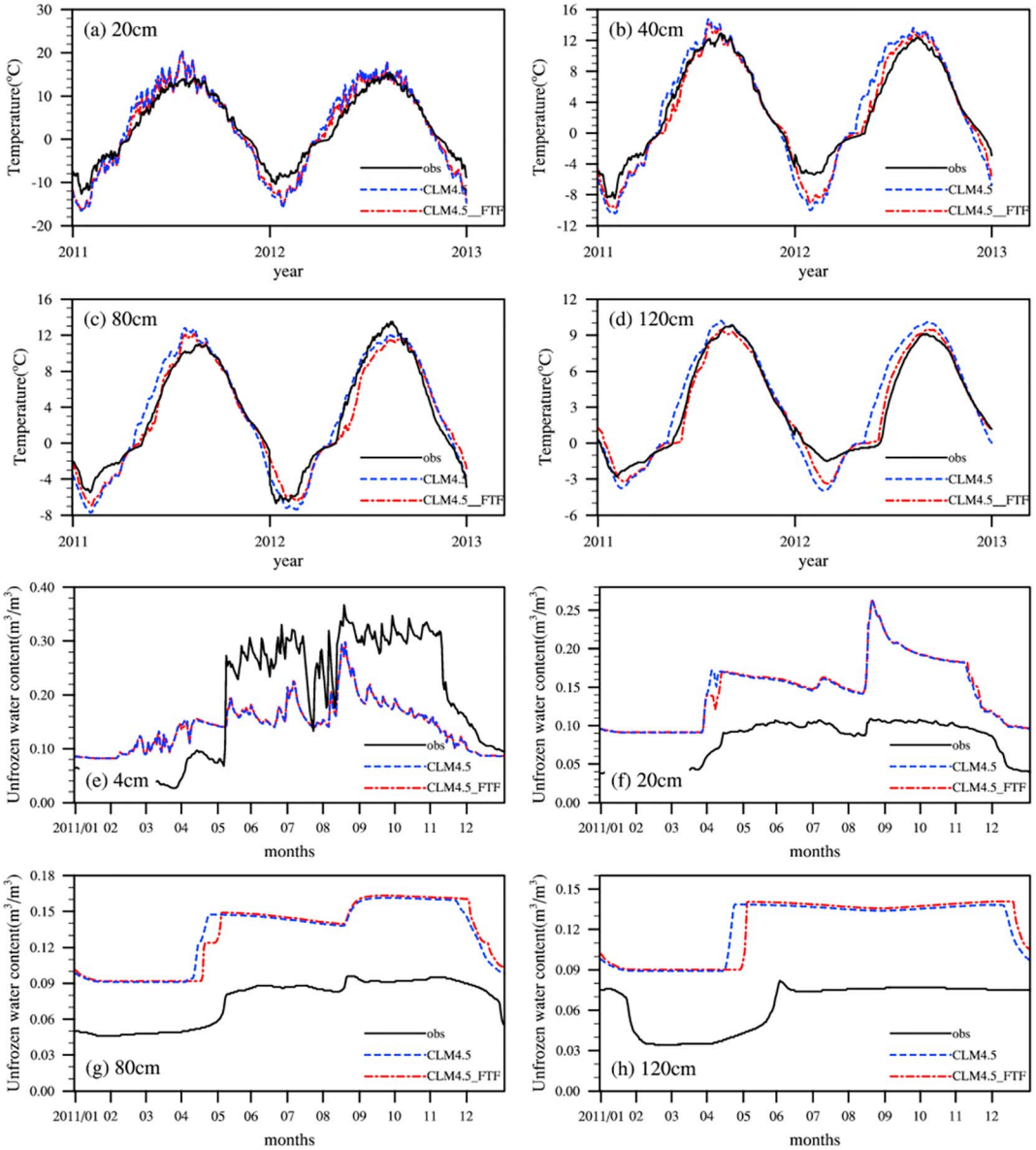

Figure 13. Observed and simulated soil temperature and soil moisture according to CLM4.5_FTF and CLM4.5 for different soil layers at the Hulugou site.

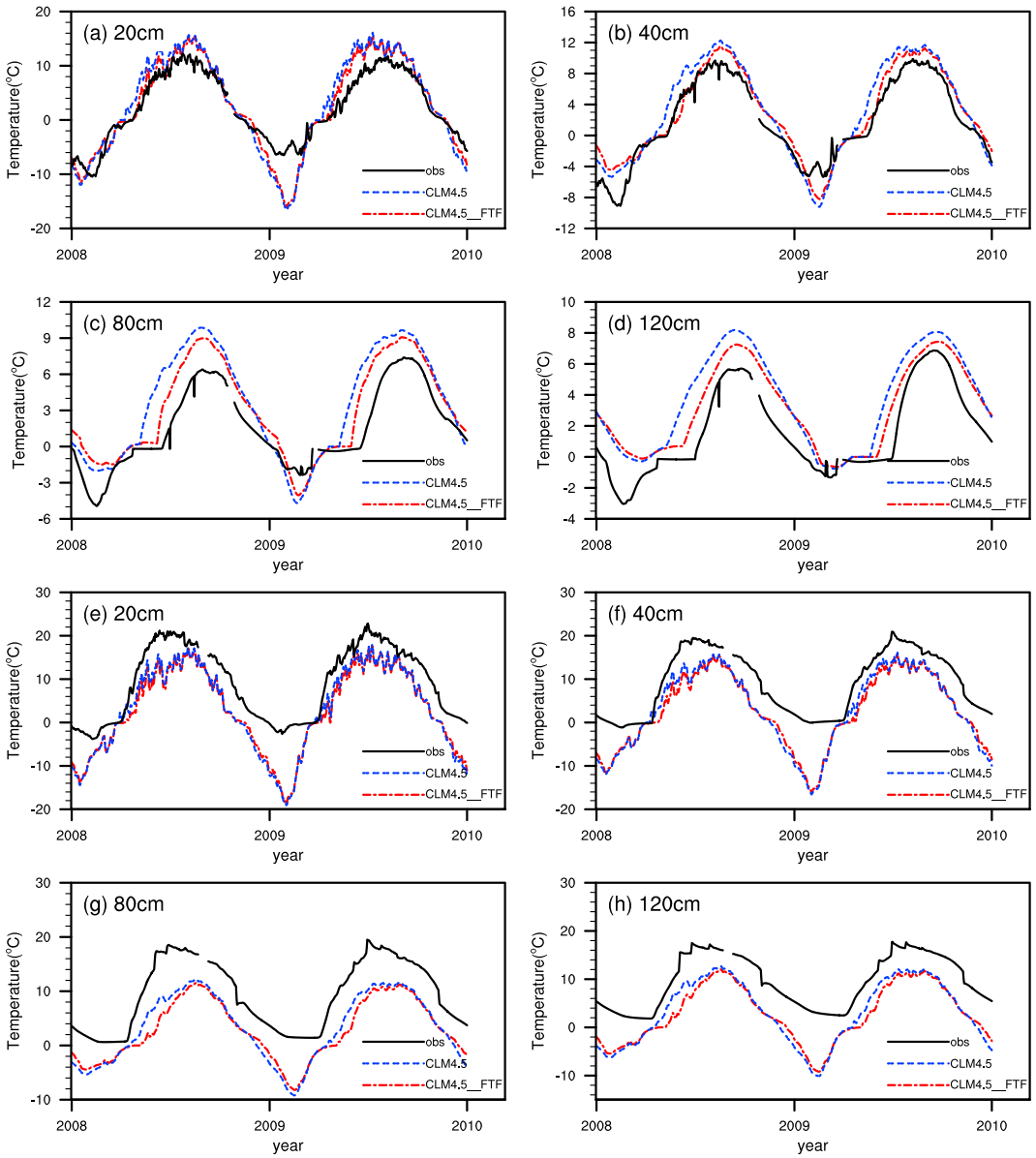

Figure 14. Observed and simulated soil temperature according to CLM4.5_FTF and CLM4.5 for different soil layers at the (a–d) Maliantan and (e–h) Yingke sites.

soil parameterization improved simulations of the soil temperature and freeze/thaw process, and the improvement was better for the lower levels than for the upper level in Hulugou and Maliantan sites, as seen in Figures 13 and 14a–14d and Tables 2 and 3. Figures 14e–14h show the observed and simulated soil temperature at Yingke site from 2008 to 2009. The results simulated by CLM4.5 and CLM4.5_FTF are both slightly less than the observed data, which may be caused by the possible inaccuracies in the atmospheric forcing data or the soil organic matter content.

Figure 15 shows the multiyear (1970–2013) mean spatial distributions of the EXP-minus-CLT difference for the latent heat flux, sensible heat flux, and 10-cm soil temperature. The maximum deviation of latent heat flux and sensible heat flux between EXP and CLT is about 4 W/m^2, and the maximum is about 1 °C for 10-cm soil temperature. There are also differences in the nonfrozen area for these variables, although the FTFs did not appear and that means the two sets of experiments have the same parameterization in these areas. It may mainly be a consequence of the surface flux change in frozen ground areas.

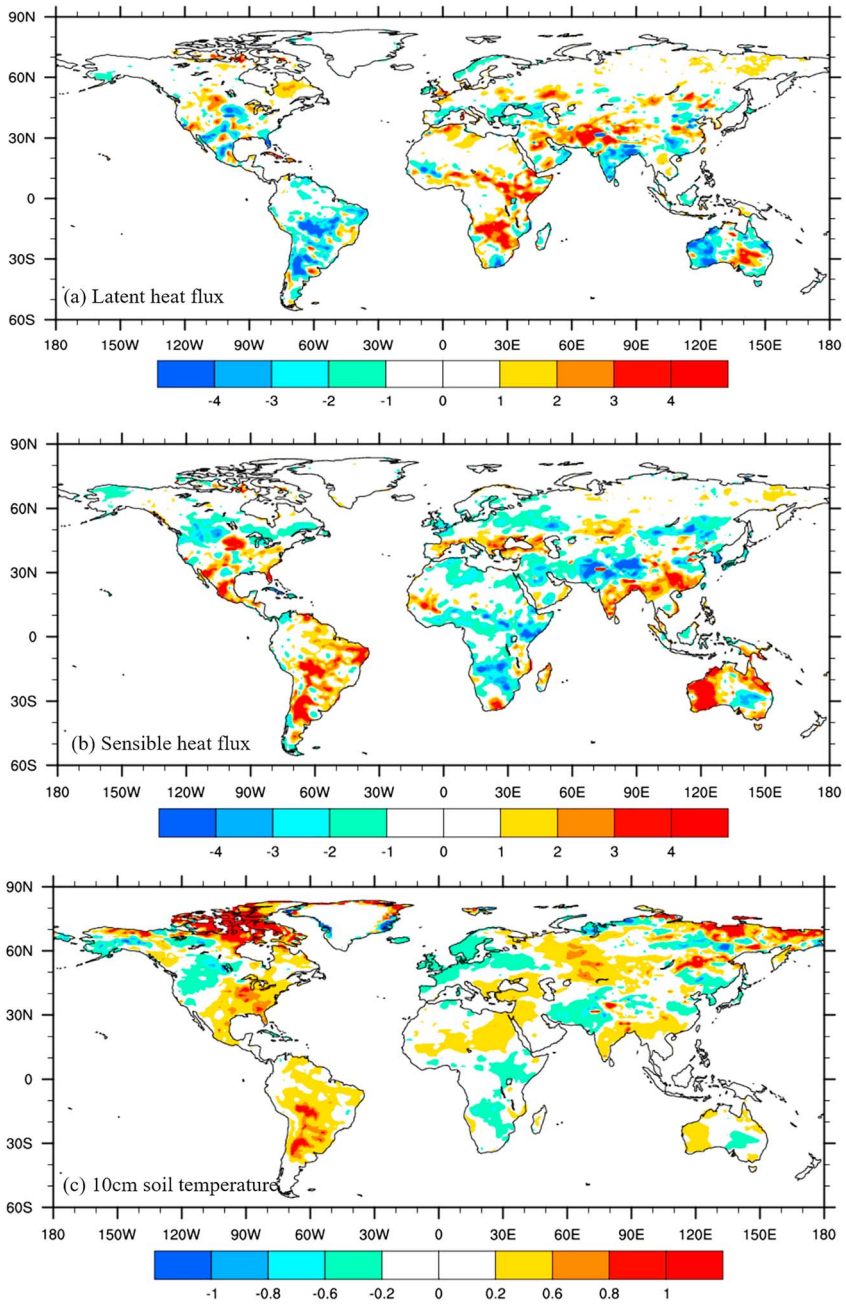

Figure 15. Spatial distribution of EXP-minus-CTL differences averaged over 1970–2013 for annual-mean (a) latent heat flux (W/m^2), (b) sensible heat flux (W/m^2), and (c) 10-cm soil temperature (°C).

6. Discussion and Conclusions

In this study, we incorporated a new frozen soil parameterization including FTF simulation into CLM4.5. We examined the performance of the new model for simulating frozen soil ground in comparison to site observations and distribution maps for frozen soil. The FTF simulations agree well with values observed at both the D66 site for permafrost and the Hulugou site for seasonally frozen ground. The maximum simulated annual thaw front depth in permafrost is defined as the ALT, and our simulated ALT values are in general agreement but slightly greater than observations from the CALM program. This is because we assume that all of the heat reaching the thaw front is used for melting soil ice, and we ignore the soil sensible heat when the soil becomes warmer during the thawing phase. Using the method described in section 2.3, we

simulated the distribution of different types of frozen soil in China and of permafrost in the Northern Hemisphere. The results agree very well with the frozen soil map of China and the IPA map. In summary, our CLM4.5_FTF model can accurately simulate the frozen ground distribution and FTFs of various sites. These results can help in decision-making for agriculture and in engineering stabilization programs for frozen ground.

The new model was then used for year-long simulations of soil temperature and soil moisture to check its applicability in continuous simulation. CLM4.5_FTF performed better than the original model for these elements, and the improvement was better for the lower levels than for the upper level in the simulations. At last, we give the simulated latent heat flux, sensible heat flux, and 10-cm soil temperature deviations determined via the couple model with and without new scheme. The differences of these variables in the nonfrozen area may mainly due to the surface flux change in frozen ground.

Some assumptions and limitations in this study should be noted. The scale mismatch in the ALT comparison may contribute to bias. The ALT comparison is based on individual site observations and mean values for the corresponding grid. Soil temperature and ALT tend to vary substantially over small distances because of the varied topography in the region (Lawrence et al., 2012). In this study, our results yielded a smaller simulated permafrost area than the IPA map (Brown et al., 1998). This is primarily attributed to the coarse horizontal resolution, which may to some extent prevent the model from capturing detailed changes in permafrost, especially at the edge of the permafrost area. In addition, the maximum FTF depth is the bottom edge of the 10 soil layers (3.8 m) because there were 10 hydrologically active soil layers and the volumetric soil water content was zero in the deeper ground layer, although the model comprised 15 soil layers to a depth of approximately 50 m. The soil column in model CLM4.5 may not be sufficient for FTF simulation (e.g., the ALT on the Tibetan Plateau may be >4.0 m). Finally, possible inaccuracies in the atmospheric forcing data, soil organic matter content, and other soil texture data may also contribute to study uncertainties.

In the future, higher-resolution atmospheric forcing data and models with finer and more accurate surface, soil organic matter, and soil texture data are required to more reasonably simulate freeze–thaw processes. We will use the new model to investigate the response of permafrost to climate change, and to examine the effects of permafrost degradation on the regional and possibly global climate in coupled land–atmosphere climate models in our ongoing work.

Acknowledgments
This work was jointly funded by the National Natural Science Foundation of China (grants 41830967 and 41575096) and the Key Research Program of Frontier Sciences, the Chinese Academy of Sciences (grant QYZDY-SSW-DQC012). The FTF depth of observed site is available at http://westdc.westgis.ac.cn/data/9a32eea2-97dc-4493-a0cd-1c1b5fd29639 and the soil temperature and soil moisture of observed site is available at http://westdc.westgis.ac.cn/data/1b6829b5-1d8f-44ae-a5a4-08f4ce3dd26a. The observed ALT data are available at https://www2.gwu.edu/~calm/data/data-links.html. The frozen ground map of China is accessible at the Cold and Arid Regions Science Data Center in China (http://westdc.westgis.ac.cn/data/6fef7011-9cac-462f-acdd-a7c43d8ddde8). The International Permafrost Association map is available at http://nsidc.org/data/docs/fgdc/ggd318_map_circumarctic/index.html. The ITP atmospheric forcing data were jointly provided by the Data Assimilation and Modeling Center for Tibetan Multi-spheres, Institute of Tibetan Plateau Research, China Academy of Sciences (http://westdc.westgis.ac.cn/data/7a35329c-c53f-4267-aa07-e0037d913a21). The model code is available upon request. Please contact Zhenghui Xie at zxie@lasg.iap.ac.cn. We would like to thank to the two reviewers for their helpful comments that improved the manuscript.

References

Anisimov, O. A., Shiklomanov, N. I., & Nelson, F. E. (1997). Global warming and active-layer thickness: Results from transient general circulation models. *Global and Planetary Change*, *15*(3–4), 61–77. https://doi.org/10.1016/S0921-8181(97)00009-X

Brown, J., Ferrians, O. J. Jr., Heginbottom, J. A., & Melnikov, E. S. (1998). *Circum-Arctic Map of Permafrost and Ground-Ice Conditions*. Boulder, CO: National Snow and Ice Data Center/World Data Center for Glaciology. *Digital media*.

Chen, R. S., Song, Y. X., Kang, E. S., Han, C. T., Liu, J. F., Yang, Y., & Liu, Z. W. (2014). A cryosphere-hydrology observation system in a small alpine watershed in the Qilian Mountains of China and its meteorological gradient. *Arctic, Antarctic, and Alpine Research*, *46*(2), 505–523. https://doi.org/10.1657/1938-4246-46.2.505

Cherkauer, K. A., & Lettenmaier, D. P. (1999). Hydrologic effects of frozen soils in the upper Mississippi River basin. *Journal of Geophysical Research*, *104*(D16), 19,599–19,610. https://doi.org/10.1029/1999JD900337

Clapp, R. B., & Hornberger, G. M. (1978). Empirical equations for some soil hydraulic properties. *Water Resources Research*, *14*(4), 601–604. https://doi.org/10.1029/WR014i004p00601

Dai, Y., Zeng, X., Dickinson, R. E., Baker, I., Bonan, G. B., Bosilovich, M. G., & Oleson, K. W. (2003). The common land model. *Bulletin of the American Meteorological Society*, *84*(8), 1013–1024. https://doi.org/10.1175/BAMS-84-8-1013

Dickinson, E., Henderson-Sellers, A., and Kennedy, J. (1993). Biosphere-Atmosphere Transfer Scheme (BATS) version 1e as coupled to the NCAR Community Climate Model.

Farouki, O. T. (1981). The thermal properties of soils in cold regions. *Cold Regions Science and Technology*, *5*(1), 67–75. https://doi.org/10.1016/0165-232X(81)90041-0

Flerchinger, G. N. (2000). *The Simultaneous Heat and Water (SHAW) Model: Technical Documentation*. Boise, Idaho: Northwest Watershed Research Center, USDA Agricultural Research Service.

Fox, J. D. (1992). Incorporating freeze-thaw calculations into a water balance model. *Water Resources Research*, *28*(9), 2229–2244. https://doi.org/10.1029/92WR00983

Frauenfeld, O. W., Zhang, T., Barry, R. G., & Gilichinsky, D. (2004). Interdecadal changes in seasonal freeze and thaw depths in Russia. *Journal of Geophysical Research*, *109*, D05101. https://doi.org/10.1029/2003JD004245

Fuchs, M., Campbell, G. S., & Papendick, R. I. (1978). An analysis of sensible and latent heat flow in a partially frozen unsaturated soil 1. *Soil Science Society of America Journal*, *42*(3), 379–385. https://doi.org/10.2136/sssaj1978.03615995004200030001x

Gao, J., Xie, Z., Wang, A., & Luo, Z. (2016). Numerical simulation based on two-directional freeze and thaw algorithm for thermal diffusion model. *Applied Mathematics and Mechanics*, *37*(11), 1467–1478. https://doi.org/10.1007/s10483-016-2106-8

Gent, P. R., Danabasoglu, G., Donner, L. J., Holland, M. M., Hunke, E. C., Jayne, S. R., & Worley, P. H. (2011). The Community Climate System Model version 4. *Journal of Climate*, *24*(19), 4973–4991. https://doi.org/10.1175/2011JCLI4083.1

Guo, D., & Wang, H. (2013). Simulation of permafrost and seasonally frozen ground conditions on the Tibetan Plateau, 1981–2010. *Journal of Geophysical Research: Atmospheres*, *118*, 5216–5230. https://doi.org/10.1002/jgrd.50457

Guo, D., & Wang, H. (2016). CMIP5 permafrost degradation projection: A comparison among different regions. *Journal of Geophysical Research: Atmospheres*, *121*, 4499–4517. https://doi.org/10.1002/2015JD024108

Harada, Y., Tsuchiya, F., Takeda, K., & Muneoka, T. (2009). Characteristics of ground freezing and thawing under snow cover based on long-term observation. *Seppyo*, *71*, 241–252.

Hurrell, J. W., Holland, M. M., Gent, P. R., Ghan, S., Kay, J. E., Kushner, P. J., & Lipscomb, W. H. (2013). The community Earth system model: A framework for collaborative research. *Bulletin of the American Meteorological Society*, *94*(9), 1339–1360. https://doi.org/10.1175/BAMS-D-12-00121.1

Iwata, Y., Hayashi, M., Suzuki, S., Hirota, T., & Hasegawa, S. (2010). Effects of snow cover on soil freezing, water movement, and snowmelt infiltration: A paired plot experiment. *Water Resources Research*, *46*, D05101. https://doi.org/10.1029/2009WR008070

Jansson, P. E. (2012). CoupModel: Model use, calibration, and validation. *Transactions of the ASABE*, *55*(4), 1337–1346. https://doi.org/10.13031/2013.42245

Jumikis, A. R. (1977). *Thermal Geotechnics* (p. 375). New Brunswick, NJ: Rutgers University Press.

Kalnay, E., Kanamitsu, M., Kistler, R., Collins, W., Deaven, D., Gandin, L., et al. (1996). The NCEP/NCAR 40-year reanalysis project. *Bulletin of the American meteorological*, *77*(3), 437–471. https://doi.org/10.1175/1520-0477(1996)077<0437:TNYRP>2.0.CO;2

Lawrence, D. M., Slater, A. G., & Swenson, S. C. (2012). Simulation of present-day and future permafrost and seasonally frozen ground conditions in CCSM4. *Journal of Climate*, *25*(7), 2207–2225. https://doi.org/10.1175/JCLI-D-11-00334.1

Li, F., Levis, S., & Ward, D. S. (2013). Quantifying the role of fire in the Earth system—Part 1: Improved global fire modeling in the Community Earth System Model (CESM1). *Biogeosciences*, *10*(4), 2293–2314. https://doi.org/10.5194/bg-10-2293-2013

Li, X., Cheng, G., Jin, H., Kang, E., Che, T., Jin, R., & Shen, Y. (2008). Cryospheric change in China. *Global and Planetary Change*, *62*(3-4), 210–218. https://doi.org/10.1016/j.gloplacha.2008.02.001

Li, X., & Koike, T. (2003). Frozen soil parameterization in SiB2 and its validation with GAME-Tibet observations. *Cold Regions Science and Technology*, *36*(1-3), 165–182. https://doi.org/10.1016/S0165-232X(03)00009-0

Lindsay, K., Bonan, G. B., Doney, S. C., Hoffman, F. M., Lawrence, D. M., Long, M. C., & Thornton, P. E. (2014). Preindustrial-control and twentieth-century carbon cycle experiments with the Earth system model CESM1 (BGC). *Journal of Climate*, *27*(24), 8981–9005. https://doi.org/10.1175/JCLI-D-12-00565.1

Lu, Q., Zhao, D., & Wu, S. (2017). Simulated responses of permafrost distribution to climate change on the Qinghai–Tibet Plateau. *Scientific Reports*, *7*(1), 3845. https://doi.org/10.1038/s41598-017-04140-7

Lunardini, V. J. (1981). Heat transfer in cold climates. Van Nostrand Reinhold Company.

Mitchell, T. D., & Jones, P. D. (2005). An improved method of constructing a database of monthly climate observations and associated high-resolution grids. *International Journal of Climatology*, *25*(6), 693–712. https://doi.org/10.1002/joc.1181

Muller, S. W. (1947). *Permafrost or Permanently Frozen Ground and Related Engineering Problems*. Burgess Hill: Edwards.

Nelson, F. E., Shiklomanov, N. I., Mueller, G. R., Hinkel, K. M., Walker, D. A., & Bockheim, J. G. (1997). Estimating active-layer thickness over a large region: Kuparuk River Basin, Alaska, U.S.A. *Arctic and Alpine Research*, *29*(4), 367–378. https://doi.org/10.2307/1551985

Niu, G. Y., & Yang, Z. L. (2006). Effects of frozen soil on snowmelt runoff and soil water storage at a continental scale. *Journal of Hydrometeorology*, *7*(5), 937–952. https://doi.org/10.1175/JHM538.1

Oleson, K., Lawrence, D., Bonan, G., Drewniak, B., Huang, M., Koven, C., et al. (2013). *Technical Description of Version 4.5 of the Community Land Model (CLM), NCAR*. Boulder, CO: National Center for Atmospheric Research (NCAR).

Pang, Q., Cheng, G., Li, S., & Zhang, W. (2009). Active layer thickness calculation over the Qinghai–Tibet Plateau. *Cold Regions Science and Technology*, *57*(1), 23–28. https://doi.org/10.1016/j.coldregions.2009.01.005

Piao, S., Ito, A., Li, S., Huang, Y., Ciais, P., Wang, X., et al. (2012). The carbon budget of terrestrial ecosystems in East Asia over the last two decades. *Biogeosciences*, *9*(9), 3571–3586. https://doi.org/10.5194/bg-9-3571-2012

Schuur, E. A., Bockheim, J., Canadell, J. G., Euskirchen, E., Field, C. B., Goryachkin, S. V., & Mazhitova, G. (2008). Vulnerability of permafrost carbon to climate change: Implications for the global carbon cycle. *AIBS Bulletin*, *58*(8), 701–714.

Schuur, E. A., Vogel, J. G., Crummer, K. G., Lee, H., Sickman, J. O., & Osterkamp, T. E. (2009). The effect of permafrost thaw on old carbon release and net carbon exchange from tundra. *Nature*, *459*(7246), 556–559. https://doi.org/10.1038/nature08031

Sellers, P. J., Randall, D. A., Collatz, G. J., Berry, J. A., Field, C. B., Dazlich, D. A., & Bounoua, L. (1996). A revised land surface parameterization (SiB2) for atmospheric GCMs. Part I: Model formulation. *Journal of Climate*, *9*(4), 676–705. https://doi.org/10.1175/1520-0442(1996)009<0676:ARLSPF>2.0.CO;2

Wang, A., Xie, Z., Feng, X., Tian, X., & Qin, P. (2014). A soil water and heat transfer model including changes in soil frost and thaw fronts. *Science China Earth Sciences*, *57*(6), 1325–1339. https://doi.org/10.1007/s11430-013-4785-0

Wang, C., & Yang, K. (2018). A new scheme for considering soil water-heat transport coupling based on Community Land Model: Model description and preliminary validation. *Journal of Advances in Modeling Earth Systems*, *10*(4), 927–950. https://doi.org/10.1002/2017MS001148

Wang, L., Koike, T., Yang, K., Jin, R., & Li, H. (2010). Frozen soil parameterization in a distributed biosphere hydrological model. *Hydrology and Earth System Sciences*, *14*(3), 557–571. https://doi.org/10.5194/hess-14-557-2010

Wang, T. (2006). 1:4000000 Map of the Glaciers, Frozen Ground and Deserts in China. Beijing: Science Press.

Woo, M. K., Arain, M. A., Mollinga, M., & Yi, S. (2004). A two-directional freeze and thaw algorithm for hydrologic and land surface modelling. *Geophysical Research Letters*, *31*, L12501. https://doi.org/10.1029/2004GL019475

Xie, C., & William, A. (2013). A simple thaw-freeze algorithm for a multi-layered soil using the Stefan equation. *Permafrost and Periglacial Processes*, *24*(3), 252–260.

Xie, Z., Liu, S., Zeng, Y., Gao, J., Qin, P., Jia, B., & Wang, L. (2018). A high-resolution land model with groundwater lateral flow, water use, and soil freeze-thaw front dynamics and its applications in an endorheic basin. *Journal of Geophysical Research: Atmospheres*, *123*, 7204–7222. https://doi.org/10.1029/2018JD028369

Xue, Y., Zeng, F. J., & Schlosser, C. A. (1996). SSiB and its sensitivity to soil properties—A case study using HAPEX-Mobilhy data. *Global and Planetary Change*, *13*(1–4), 183–194. https://doi.org/10.1016/0921-8181(95)00045-3

Yang, K., He, J., Tang, W., Qin, J., & Cheng, C. C. (2010). On downward shortwave and longwave radiations over high altitude regions: Observation and modeling in the Tibetan Plateau. *Agricultural and Forest Meteorology*, *150*(1), 38–46. https://doi.org/10.1016/j.agrformet.2009.08.004

Yi, S., Arain, M. A., & Woo, M. K. (2006). Modifications of a land surface scheme for improved simulation of ground freeze-thaw in northern environments. *Geophysical Research Letters*, *33*, L13501. https://doi.org/10.1029/2006GL026340

Zeng, Y., Xie, Z., & Liu, S. (2017). Seasonal effects of irrigation on land–atmosphere latent heat, sensible heat and carbon fluxes in semi-arid basin. *Earth System Dynamics*, *8*(1), 113–127. https://doi.org/10.5194/esd-8-113-2017

Zeng, Y., Xie, Z., Liu, S., Xie, J., Jia, B., Qin, P., & Gao, J. (2018). Global land surface modeling including lateral groundwater flow. *Journal of Advances in Modeling Earth Systems*, *10*(8), 1882–1900. https://doi.org/10.1029/2018MS001304

Zeng, Y., Xie, Z., Yu, Y., Liu, S., Wang, L., Jia, B., et al. (2016a). Ecohydrological effects of stream–aquifer water interaction: A case study of the Heihe River basin, northwestern China. *Hydrology and Earth System Sciences*, *20*(6), 2333–2352. https://doi.org/10.5194/hess-20-2333-2016

Zeng, Y., Xie, Z., Yu, Y., Liu, S., Wang, L., Zou, J., et al. (2016b). Effects of anthropogenic water regulation and groundwater lateral flow on land processes. *Journal of Advances in Modeling Earth Systems*, *8*, 1106–1131. https://doi.org/10.1002/2016MS000646

Zeng, Y., Xie, Z., & Zou, J. (2017). Hydrologic and climatic responses to global anthropogenic groundwater extraction. *Journal of Climate*, *30*(1), 71–90. https://doi.org/10.1175/JCLI-D-16-0209.1

Zhang, T. (2005). Influence of the seasonal snow cover on the ground thermal regime: An overview. *Reviews of Geophysics*, *43*, RG4002. https://doi.org/10.1029/2004RG000157

Zhang, T., Barry, R. G., Knowles, K., Heginbottom, J. A., & Brown, J. (1999). Statistics and characteristics of permafrost and ground-ice distribution in the Northern Hemisphere 1. *Polar Geography*, *23*(2), 132–154. https://doi.org/10.1080/10889379909377670

Zhang, Z., & Wu, Q. (2012). Predicting changes of active layer thickness on the Qinghai-Tibet plateau as climate warming (in Chinese). *Journal of Glaciology and Geocryology*, *34*(3), 505–511.

Zhuang, Q., Melillo, J. M., Kicklighter, D. W., Prinn, R. G., McGuire, A. D., Steudler, P. A., & Hu, S. (2004). Methane fluxes between terrestrial ecosystems and the atmosphere at northern high latitudes during the past century: A retrospective analysis with a process-based biogeochemistry model. *Global Biogeochemical Cycles*, *18*, GB3010. https://doi.org/10.1029/2004GB002239

Zimov, S. A., Schuur, E. A., & Chapin, F. S. (2006). Permafrost and the global carbon budget. *Science*, *312*(5780), 1612–1613. https://doi.org/10.1126/science.1128908